

Phase diagram, confining strings, and a new universality class in nematopolar matter

Farzan Vafa^{1,2} and Amin Doostmohammadi³

¹*Center of Mathematical Sciences and Applications,
Harvard University, Cambridge, MA 02138, USA*

²*Physics of Living Systems, Department of Physics,
Massachusetts Institute of Technology, Cambridge, Massachusetts 02139, USA*

³*Niels Bohr Institute, University of Copenhagen, Blegdamsvej 17, Copenhagen 2100, Denmark*

(Dated: January 10, 2025)

We study a minimal model of a system with coexisting nematic and polar orientational orders, where one field tends to order and the other prefers isotropy. For strong coupling, the ordered field aligns the isotropic one, locking their orientations. The phase diagram reveals three distinct phases—nematopolar (aligned orders), nematic (independent orders), and isotropic (vanishing orders)—separated by continuous and discontinuous transitions, including a triple and a tricritical point. We find unique critical scaling for the nematopolar-nematic transition, distinct from standard nematic or polar universality classes. Additionally, in the locked nematopolar phase, we show nematic $+1/2$ topological defect pairs are connected and confined by *strings* with constant tension. These strings arise from frustration in locking the orientational orders and can be interpreted as elongated cores of $+1$ polar topological defects. When a sufficiently strong background field couples to the polar order, all topological defects are expelled from the region. Analytical predictions are quantitatively confirmed by numerical simulations.

Oriental order, characterized by the alignment of constituent units in preferred directions, is a fundamental phenomenon observed across a wide range of natural and synthetic systems [1]. This order manifests in various forms, from the liquid crystals in display technologies (LCDs) [2] to the collective behaviors seen in biological tissues [3]. Common examples include polar order, where units align in a specific direction, akin to the coordinated movement of a flock of birds [4] or the arrangement of molecules in Langmuir-Blodgett monolayers at a liquid-air interface [5]. Similarly, nematic order is observed when units align along a common axis, as seen in liquid crystal sensors [6], nematic elastomers [7], bacterial aggregates [8, 9], suspensions of cytoskeletal filaments and associated motor proteins [10], or in epithelial monolayers [11].

In many real-world materials, these types of orientational order do not exist in isolation but often coexist and interact, leading to complex phases. Recent studies have uncovered phases such as the ferroelectric nematic phase [12–14], where polar molecules with strong dipole moments exhibit both polar and nematic order, and the hexanematic phase, observed in Madin-Darby canine kidney cells, which displays both nematic and hexatic order [15–17]. A well-studied example of such coexistence is the tilted hexatic phase, which combines polar and hexatic order [18–22]. Similarly, a model of hexatic-nematic order coupling has been studied recently and found strings connecting three $+1/6$ hexatic topological defects, as well as an extended nematic $+1/2$ defect that connects the hexatic defects [23]. These discoveries highlight the rich interplay between different types of orientational order in various physical systems, from synthetic liquid crystals to biological tissues, underscoring the importance of understanding these interactions

for both fundamental science and practical applications.

Previous studies of coupled distinct order parameters have focused on the case of coupled scalar or vector order parameters [24] and primarily on coupling the phases of orientational orders with fixed magnitudes [18, 21–23], including gradient couplings as in flexoelectricity [14, 25–

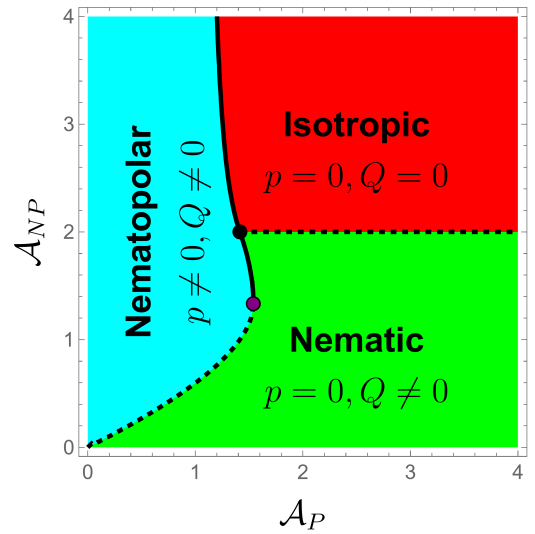


FIG. 1. Phase diagram of a system with coexisting nematic and polar orders. The solid lines mark first order phase transitions, and the dashed lines are second order phase transitions. The tricritical point (purple filled circle) is at $(\mathcal{A}_P, \mathcal{A}_{NP}) = (8/\sqrt{27}, 4/3)$, and the triple point (black filled circle) is at $(\mathcal{A}_P, \mathcal{A}_{NP}) = (\sqrt{2}, 2)$. The dashed phase boundary connecting the origin to the white point satisfies Eq. (4). The other dashed phase boundary is given by $\mathcal{A}_{NP} = 2$ for $\mathcal{A}_P > \sqrt{2}$. The lower and upper segments of the solid phase boundary satisfy Eqs. (S.23) and (S.28), respectively.

30], as well as polar and nematic-like interactions of a single field [31–35].

In this work, we propose a minimal theory that couples both the phase and magnitude of nematic and polar order parameters and captures interactions between distinct nematic and polar fields. As we shall show, structural implications of accounting for this physical effect are drastic.

A minimal nematopolar model. The three main contributions to the minimal nematopolar free energy that we consider are: (i) \mathcal{F}_p , an isotropic polar free energy, where the polar order parameter \vec{p} has inherent tendency to be isotropic (ii) \mathcal{F}_Q , ordered nematic free energy, where the nematic order parameter \overleftrightarrow{Q} (traceless symmetric rank-2 tensor) has inherent tendency to be ordered (iii) \mathcal{F}_c , a coupling which tends to align the polar and nematic order parameters.¹ Then the total free energy \mathcal{F} is the sum of these three contributions, with $\mathcal{F}[\vec{p}, \overleftrightarrow{Q}] = \mathcal{F}_p[\vec{p}] + \mathcal{F}_Q[\overleftrightarrow{Q}] + \mathcal{F}_c[\vec{p}, \overleftrightarrow{Q}]$, where

$$\mathcal{F}_p = \int d^2z [K_p |\nabla \vec{p}|^2 + \mathcal{A}_P |\vec{p}|^2] \quad (1a)$$

$$\mathcal{F}_Q = \int d^2z [K_Q |\nabla \cdot \overleftrightarrow{Q}|^2 + \mathcal{A}_Q (1 - |Q|^2)^2] \quad (1b)$$

$$\mathcal{F}_c = \mathcal{A}_{NP} \int d^2z |\overleftrightarrow{Q} - \overleftrightarrow{P}|^2, \quad (1c)$$

where explicitly for notational convenience, $|\nabla \vec{p}|^2 \equiv (\partial_i p^j)^2$, $|\vec{p}|^2 \equiv p_i p^i$, $|\nabla \cdot \overleftrightarrow{Q}|^2 \equiv (\partial_i Q^{ij})^2$, $|Q|^2 \equiv \text{tr}[\overleftrightarrow{Q}^2]$, $\overleftrightarrow{P} \equiv \vec{p}\vec{p} - (|\vec{p}|^2/2)\overleftrightarrow{1}$, and $|\overleftrightarrow{Q} - \overleftrightarrow{P}|^2 \equiv \text{tr}[(\overleftrightarrow{Q} - \overleftrightarrow{P})^2]$.

In \mathcal{F}_p , the polar elasticity $K_p > 0$, with units of energy, defines the energetic cost of spatial variations of \vec{p} , while the disorder parameter $\mathcal{A}_P > 0$, with units of energy density, controls the strength of the polar order via the coherence length $w = \sqrt{K_p/\mathcal{A}_P}$, which governs spatial variations in the magnitude of \vec{p} . Similarly, in \mathcal{F}_Q , the nematic elasticity $K_Q > 0$, with units of energy, defines the energetic cost of spatial variations of \overleftrightarrow{Q} , and the order parameter $\mathcal{A}_Q > 0$, with units of energy density, controls the strength of the nematic order. By inspection of Eqs. (1a) and (1b), $\vec{p} = 0$ minimizes \mathcal{F}_p and homogeneous \overleftrightarrow{Q} with magnitude $|Q| = 1$ minimizes \mathcal{F}_Q .

In \mathcal{F}_c , the aligning parameter $\mathcal{A}_{NP} > 0$, with units of energy density, defines the energetic cost of misalignment between \overleftrightarrow{Q} and \overleftrightarrow{P} . By inspection of Eq. (1c), $\overleftrightarrow{Q} = \overleftrightarrow{P}$

minimizes \mathcal{F}_c . The total free energy \mathcal{F} is thus

$$\mathcal{F}[p, Q] = \int d^2z \left[\mathcal{A}_{NP} \left| \overleftrightarrow{Q} - \overleftrightarrow{P} \right|^2 + \mathcal{A}_P |\vec{p}|^2 + \mathcal{A}_Q (1 - |Q|^2)^2 + K_p |\nabla \vec{p}|^2 + K_Q |\nabla \cdot \overleftrightarrow{Q}|^2 \right]. \quad (2)$$

Without loss of generality, the polar vector \vec{p} is assumed to align along the x -direction with magnitude p , while the nematic order parameter \overleftrightarrow{Q} is aligned with the polar order with magnitude Q , and both are homogeneous. The free energy is then expressed as

$$\mathcal{F} = \mathcal{A}_{NP} (Q - p^2)^2 + \mathcal{A}_P p^2 + \mathcal{A}_Q (1 - Q^2)^2, \quad (3)$$

where \mathcal{A}_P , \mathcal{A}_Q , and \mathcal{A}_{NP} represent contributions from polar disorder, nematic order, and polar-nematic coupling, respectively. By rescaling \mathcal{F} , we set $\mathcal{A}_Q = 1$ without loss of generality.

The competition between the three terms leads to three distinct phases, as shown in the phase diagram (Fig. 1). The \mathcal{A}_P term suppresses polar order ($p = 0$), the \mathcal{A}_Q term favors maximal nematic order ($Q = 1$), and the \mathcal{A}_{NP} term couples Q and p via $Q = p^2$. Two limiting cases provide insight into the phase behavior: (i) $\mathcal{A}_{NP} \gg 1$ and (ii) $\mathcal{A}_P \gg 1$.

(i) For $\mathcal{A}_{NP} \gg 1$, the coupling enforces $Q \sim p^2$. When \mathcal{A}_P is large, $p = 0$ and $Q = 0$, corresponding to the isotropic phase (red region, Fig. 1). For small \mathcal{A}_P ($\mathcal{A}_P < 4\sqrt{6}/9$), nematic ordering dominates, leading to $Q \neq 0$ and $Q \sim p^2 \neq 0$, defining the nematopolar phase (cyan region). These phases are separated by a first-order phase transition (solid curve), asymptoting to $\mathcal{A}_P = 4\sqrt{6}/9$.

(ii) For $\mathcal{A}_P \gg 1$, polar disorder dominates, yielding $p = 0$. If \mathcal{A}_{NP} exceeds 2, the system remains isotropic ($Q = p^2 = 0$). For $\mathcal{A}_{NP} < 2$, nematic order emerges ($Q \neq 0, p = 0$), defining the nematic phase (green region). The isotropic and nematic phases are separated

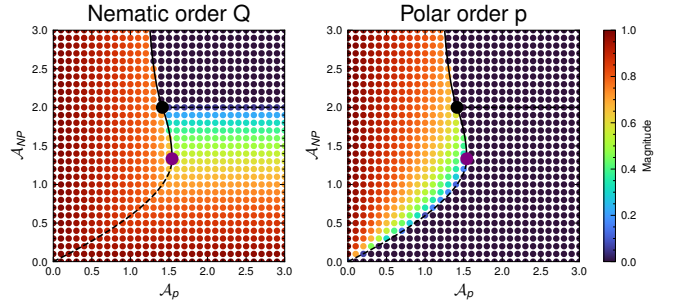


FIG. 2. Phase diagram obtained from numerical simulations. Left panel: plot of $|Q|$. Right panel: plot of $|p|$. Each marker is a simulation result. Analytical phase boundaries are superimposed on top, where the solid lines are discontinuous phase transitions, and the dashed lines are continuous phase transitions.

¹ A related polarnematic model, where the roles of \vec{p} and \overleftrightarrow{Q} are switched, i.e., \vec{p} is ordered and \overleftrightarrow{Q} isotropic, is analyzed in the Supplemental Material.

	α	β	γ
N \rightarrow I: Q	0	1/2	1
NP \rightarrow N: p	(0, 1)	(1/2, 1/4)	(1, 1/2)
N \rightarrow NP: σ	0	1	0

TABLE I. Mean-field critical exponents. The critical exponents α , β , and γ are defined by specific heat $C \equiv -T \frac{\partial^2 \mathcal{F}}{\partial T^2} \propto (T - T^*)^{-\alpha}$, magnetization $m \propto (T - T^*)^\beta$, and susceptibility $\chi \equiv \frac{\partial m}{\partial h} \Big|_{h=0} \propto (T - T^*)^{-\gamma}$, respectively, where h is an external field. The second entries for p denote the shifted values at the tricritical point.

by a continuous transition (dashed line, Fig. 1), which satisfies $\mathcal{A}_{NP} = 2$ for $\mathcal{A}_P \geq \sqrt{2}$.

The nematopolar and nematic phases are delineated by a boundary comprising a continuous transition (dashed curve, origin to purple tricritical point) and a first-order transition (solid curve, tricritical to black triple point). The dashed boundary satisfies

$$2\mathcal{A}_{NP}\sqrt{1 - \mathcal{A}_{NP}/2} = \mathcal{A}_P, \quad (4)$$

with the critical $\mathcal{A}_{NP}^*(\mathcal{A}_P)$ defined as its smallest positive solution. The analytical results are corroborated by numerical simulations in Fig. 2, with details in the Supplemental Material.

Critical exponents and a new universality class.

The phases and phase transitions identified are characterized by analytically obtained mean-field critical exponents for the N-I and N-NP continuous phase transitions, summarized in Table I (see the Supplemental Material for derivations). The critical exponents α , β , and γ describe the behavior of the specific heat $C \equiv -T \partial^2 \mathcal{F} / \partial T^2 \propto (T - T^*)^{-\alpha}$, the order parameter $m \propto (T - T^*)^\beta$, and the susceptibility $\chi \equiv \partial m / \partial h \Big|_{h=0} \propto (T - T^*)^{-\gamma}$, where h is an external field.

For the N-I phase boundary, the scaling $2 - \mathcal{A}_{NP} \approx T^* - T$ is assumed, with $m = Q$. This yields critical exponents identical to the mean-field Ising model: $\alpha = 0$, $\beta = 1/2$, and $\gamma = 1$. For the N-NP phase boundary, the scaling $\mathcal{A}_P^* - \mathcal{A}_P \approx T - T^*$ is used, with two relevant order parameters: p and the locking order parameter $\sigma \equiv Q - p^2 - \mathcal{A}_P / (2\mathcal{A}_{NP})$, where $\sigma = 0$ in the nematopolar phase.

Generically, p exhibits critical exponents $\alpha = 0$, $\beta = 1/2$, and $\gamma = 1$. At the tricritical point $(\mathcal{A}_P, \mathcal{A}_{NP}) = (8/\sqrt{27}, 4/3)$, these exponents shift to $\alpha = 1$, $\beta = 1/4$, and $\gamma = 1/2$. For σ , the exponents are $\alpha = 0$, $\beta = 1$, and $\gamma = 0$. Notably, these exponents for the N-NP boundary do not correspond to standard universality classes of nematic or polar matter.

The change in α at the tricritical point reflects the discontinuity of $\partial^2 \mathcal{F} / \partial T^2$ across the transition. This finding highlights the unconventional nature of critical

phenomena in the system and underscores the richness of the underlying phase structure.

Confining strings. Having established the distinct ordered phases and their transitions, we analyze the behavior of topological defects, where order breaks down. For analytical clarity, we focus on isolated defects. Consider a configuration with a +1 polar defect and a pair of +1/2 nematic defects (not necessarily bound). In nematics, +1 defects decompose into pairs of +1/2 defects due to Coulomb repulsion. For polar order, however, the elementary defect charge is +1. If nematic order \vec{Q} is strongly coupled to polar order \vec{p} , such that $\vec{Q} \approx \vec{p}$, a +1 polar defect induces a minimal +1 nematic defect, leading to confinement of +1/2 nematic defects. The strength of this confinement depends on the coupling parameter \mathcal{A}_{NP} .

In the strongly locked regime ($\mathcal{A}_{NP} \gg \mathcal{A}_{NP}^*$), $\vec{Q} \approx \vec{p}$, confining +1/2 nematic defects. In the weakly locked regime ($\mathcal{A}_{NP} \gtrsim \mathcal{A}_{NP}^*$), frustration emerges between nematic and polar fields. This frustration localizes along a string connecting the +1/2 defects, where \vec{p} becomes ordered, resulting in a stretched defect core. The string has a characteristic width w , corresponding to the polar coherence length, and a length ℓ , determined by minimizing the free energy.

The free energy components include the nematic elastic term

$$\mathcal{F}_Q = \frac{\pi}{2} K_Q \ln(L/\ell), \quad (5)$$

where L is the system size, and the combined contributions of polar and coupling energies, given by $\mathcal{F}_c + \mathcal{F}_p \sim f(\mathcal{A}_{NP})w\ell$. For $\mathcal{A}_{NP} \gg 1$, $f(\mathcal{A}_{NP}) \sim \mathcal{A}_{NP}$. Near the N-NP curve, the string tension must vanish, requiring $f(\mathcal{A}_{NP}) \sim \mathcal{A}_{NP} - \mathcal{A}_{NP}^*(\mathcal{A}_P)$, where $\mathcal{A}_{NP}^*(\mathcal{A}_P)$ lies on the N-NP curve. Using $w = \sqrt{K_p/\mathcal{A}_P}$, the string tension is

$$T \equiv (\mathcal{A}_{NP} - \mathcal{A}_{NP}^*) \sqrt{\frac{K_p}{\mathcal{A}_P}}. \quad (6)$$

Replacing this into the total free energy

$$\mathcal{F} \sim \frac{\pi}{2} K_Q \ln(L/\ell) + T\ell, \quad (7)$$

and minimizing with respect to the string length ℓ gives

$$\ell \sim \frac{\pi}{2} \sqrt{\frac{K_Q^2 \mathcal{A}_P}{K_p}} \frac{1}{\mathcal{A}_{NP} - \mathcal{A}_{NP}^*}. \quad (8)$$

Numerical simulations confirm these predictions, as shown in Fig. 3. Panels (b) and (c) illustrate steady-state configurations in the confined and deconfined regimes, respectively. Panel (d) measures the equilibrium string length ℓ , and Fig. 3(e-f) verifies the theoretical scaling for

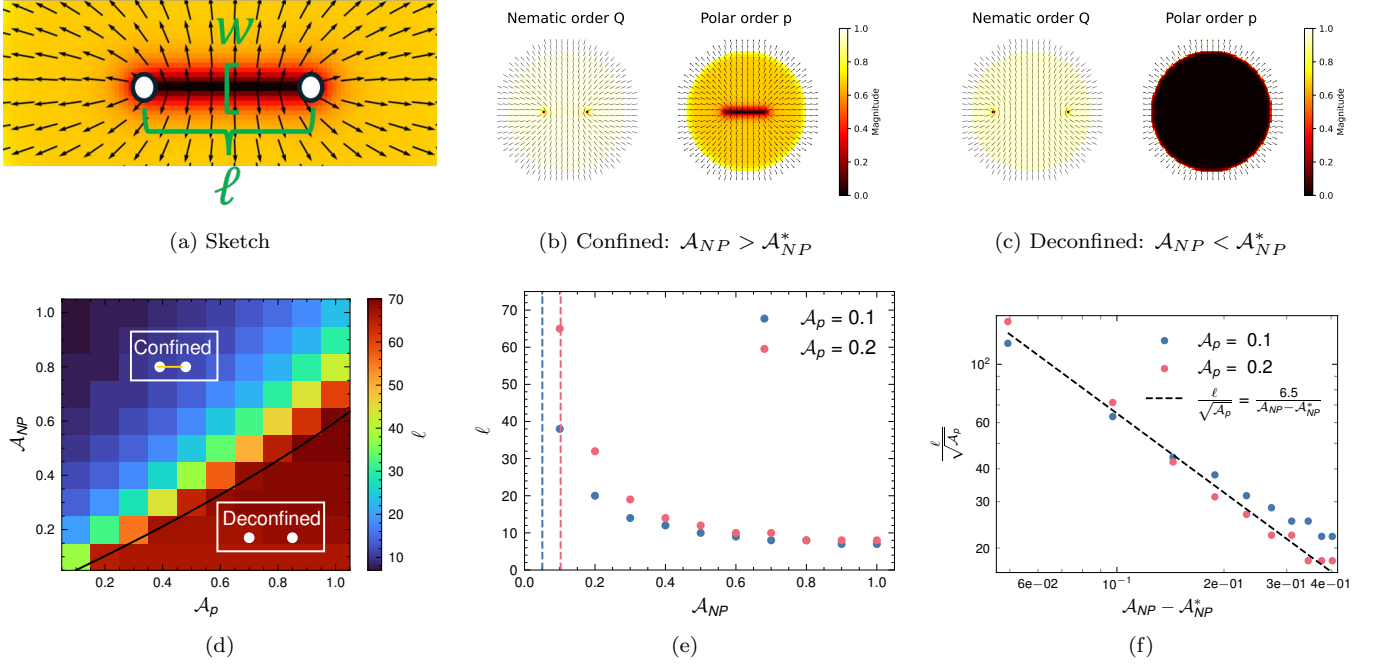


FIG. 3. Confining strings. (a) Sketch of elongated +1 polar defect of length ℓ and width w . A pair of +1/2 defects, at the endpoints of the string, are confined. (b) and (c) Stationary plots of p and Q where color denotes the magnitude for (b) confined regime ($\mathcal{A}_P = 0.1$ and $\mathcal{A}_{NP} = 0.1$) and (c) deconfined regime ($\mathcal{A}_P = 1.0$ and $\mathcal{A}_{NP} = 0.1$). (d) Phase diagram with data from numerical simulations of confinement/deconfinement transition, where color indicates separation distance ℓ of the two +1/2 defects. Insets indicate parameter region of confined and deconfined defects. (e) and (f) Plots of equilibrium length ℓ of bound pairs of +1/2 defects for small values of \mathcal{A}_P . (e) Colored dashed vertical lines denote \mathcal{A}_{NP}^* . (f) Log-log plot, where red dashed line is fit of Eq. (8).

small \mathcal{A}_P . These findings reveal how defect confinement arises from the interplay between polar and nematic orders, with implications for understanding topological excitations in systems with coexisting orientational orders.

Unlike recent experimental observations of strings connecting neutral nematic defect pairs in endothelial cell layers [36], our model reveals the confinement of same-sign nematic defects. A neutral nematic defect pair in the nematopolar phase would similarly form a string, but this configuration is unstable due to the combined effect of Coulombic and string tension forces, which are both attractive. In contrast, for same-sign defects, the Coulombic repulsion opposes the string tension, resulting in a stable equilibrium. This key distinction offers fresh insights into the stabilization mechanisms of topological defects and raises intriguing questions about the potential role of external fields or other perturbations in stabilizing strings for neutral defect pairs.

Coupling to External Fields. The impact of external fields on the system is examined by coupling \overleftrightarrow{Q} and \vec{p} to fields \overleftrightarrow{H} and \vec{h} , respectively, through the following free

energy:

$$\mathcal{F} = \mathcal{A}_{NP} \left| \overleftrightarrow{Q} - \overleftrightarrow{P} \right|^2 + \mathcal{A}_P |p|^2 + (|Q|^2 - 1)^2 - \text{tr} \left[\overleftrightarrow{H} \overleftrightarrow{Q} \right] - \vec{h} \cdot \vec{p}. \quad (9)$$

Two cases are considered: (i) $\vec{h} = 0$, $\overleftrightarrow{H} \neq 0$, and (ii) $\vec{h} \neq 0$, $\overleftrightarrow{H} = 0$ (see the Supplemental Material for derivations).

(i) When $\vec{h} = 0$, the free energy is minimized when \overleftrightarrow{H} , \overleftrightarrow{Q} , and \overleftrightarrow{P} are all aligned. Non-zero external field \overleftrightarrow{H} prohibits $\overleftrightarrow{Q} = 0$ as a solution, eliminating the nematic-isotropic (N-I) phase boundary. However, both $\vec{p} = 0$ and $\vec{p} \neq 0$ remain valid solutions, preserving the continuity of the nematic-nematopolar (N-NP) phase boundary, albeit in a deformed form.

(ii) When $\overleftrightarrow{H} = 0$, the free energy is minimized when \vec{p} aligns with \vec{h} and \overleftrightarrow{Q} aligns with \overleftrightarrow{P} . Here, non-zero \vec{h} prohibits $\vec{p} = 0$ as a solution, thereby also excluding $\overleftrightarrow{Q} = 0$. As a result, the nematic and isotropic phases are no longer stable, and only the nematopolar phase persists.

The fate of topological defects in the presence of a large external field \vec{h} is particularly intriguing. Consider a region where \vec{h} points in the $+\hat{x}$ direction. For a +1 polar aster defect at the origin, the field p^x changes sign

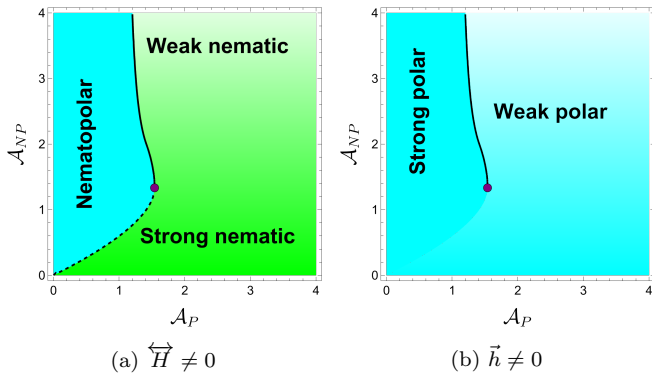


FIG. 4. Schematic phase diagrams in the presence of external fields. (a) \vec{Q} is coupled to small external field $\vec{H} \neq 0$. The N-I phase boundary disappears, but the other phase boundaries remain, but deformed. (b) \vec{p} is coupled to small external field $\vec{h} \neq 0$. Both continuous phase boundaries disappear, leaving only a single ordered phase.

across $x = 0$, leading to an asymmetric energy contribution. In the region $x > 0$, \vec{p} aligns with \vec{h} and thus lowers the energy, whereas in the region $x < 0$, \vec{p} misaligns and thus raises the energy. This energy asymmetry induces a force on the defect, driving it in the $-x$ direction to align with \vec{h} . Thus, external fields render defects mobile and, for sufficiently large \vec{h} , repel them entirely (see the Supplemental Material for representative snapshots of movement of the topological defects). This result highlights the profound influence of external fields in suppressing topological defects, fundamentally altering the phase behavior and providing new avenues to control systems with coexisting orientational orders.

Discussion. Introducing a minimal nematopolar model that captures the coupling between polar and nematic order, and through analytical calculations, we uncovered a rich phase diagram featuring nematopolar, nematic, and isotropic phases, with phase transitions characterized by distinct critical exponents that do not fall under any known universality classes. These theoretical findings were validated by extensive numerical simulations.

The nematopolar phase presents dual and complementary perspectives: (i) nematic order induces polar order, and (ii) a polar $+1$ defect confines a pair of nematic $+1/2$ defects. In this confined phase, the $+1/2$ defects are connected by a string with a well-defined tension, proportional to $\mathcal{A}_{NP} - \mathcal{A}_{NP}^*$. This string stabilizes the defect pair, and its equilibrium length ℓ scales as $\ell \sim 1/(\mathcal{A}_{NP} - \mathcal{A}_{NP}^*)$. Such confinement and string formation underscore the intricate coupling between polar and nematic fields and provide a novel mechanism for defect stabilization in active and passive systems.

Our findings highlight the rich phenomenology that emerges from the interplay between nematic and polar

orientational order, offering new insights into systems with competing symmetries. The identification of distinct phases and critical behaviors, including novel universality at the nematopolar-nematic transition, broadens the landscape of phase transitions in soft and active matter. The identification of string-mediated confinement of nematic defects in the nematopolar phase provides a striking example of frustration-driven defect interactions, with potential implications for the design and control of defect networks in liquid crystals and active materials. Collectively, these results pave the way for understanding how coupled orientational fields shape collective behavior in diverse soft matter systems, with potential applications ranging from liquid crystal technologies to biological systems with intrinsic order.

ACKNOWLEDGMENTS

It is a pleasure to acknowledge helpful conversations with Aboutaleb Amiri, Jonathan Bauermann, Lara Braverman, Nikta Fakhri, Luca Giomi, Mehran Kardar, and David Nelson. This work is partially supported by the Center for Mathematical Sciences and Applications at Harvard University (F. V.). F.V. gratefully acknowledges the Niels Bohr Institute for their hospitality, where some of the research for this paper was performed. A. D. acknowledges funding from the Novo Nordisk Foundation (grant No. NNF18SA0035142 and NERD grant No. NNF21OC0068687), Villum Fonden (Grant no. 29476), and the European Union (ERC, PhysCoMeT, 101041418). Views and opinions expressed are however those of the authors only and do not necessarily reflect those of the European Union or the European Research Council. Neither the European Union nor the granting authority can be held responsible for them.

-
- [1] P. G. de Gennes and J. Prost, *The physics of liquid crystals* (Clarendon Press, Oxford, 1993).
 - [2] D.-K. Yang and S.-T. Wu, *Fundamentals of liquid crystal devices* (John Wiley & Sons, 2014).
 - [3] A. Doostmohammadi and B. Ladoux, *Physics of liquid crystals in cell biology*, Trends in cell biology (2021).
 - [4] M. C. Marchetti, J.-F. Joanny, S. Ramaswamy, T. B. Liverpool, J. Prost, M. Rao, and R. A. Simha, Hydrodynamics of soft active matter, *Reviews of modern physics* **85**, 1143 (2013).
 - [5] V. M. Kaganer, H. Möhwald, and P. Dutta, Structure and phase transitions in langmuir monolayers, *Reviews of Modern Physics* **71**, 779 (1999).
 - [6] A. Schenning, G. P. Crawford, and D. J. Broer, *Liquid crystal sensors* (CRC Press, 2017).
 - [7] S. W. Ula, N. A. Traugutt, R. H. Volpe, R. R. Patel, K. Yu, and C. M. Yakacki, Liquid crystal elastomers: an

- introduction and review of emerging technologies, *Liquid Crystals Reviews* **6**, 78 (2018).
- [8] D. Volfson, S. Cookson, J. Hasty, and L. S. Tsimring, Biomechanical ordering of dense cell populations, *Proceedings of the National Academy of Sciences* **105**, 15346 (2008).
- [9] A. Doostmohammadi, S. P. Thampi, and J. M. Yeomans, Defect-mediated morphologies in growing cell colonies, *Physical review letters* **117**, 048102 (2016).
- [10] K. Kruse, J.-F. Joanny, F. Jülicher, J. Prost, and K. Sekimoto, Generic theory of active polar gels: a paradigm for cytoskeletal dynamics, *The European Physical Journal E* **16**, 5 (2005).
- [11] T. B. Saw, A. Doostmohammadi, V. Nier, L. Kocgozlu, S. Thampi, Y. Toyama, P. Marcq, C. T. Lim, J. M. Yeomans, and B. Ladoux, Topological defects in epithelia govern cell death and extrusion, *Nature* **544**, 212–216 (2017).
- [12] X. Chen, E. Korblova, D. Dong, X. Wei, R. Shao, L. Radzihovsky, M. A. Glaser, J. E. MacLennan, D. Bedrov, D. M. Walba, *et al.*, First-principles experimental demonstration of ferroelectricity in a thermotropic nematic liquid crystal: Polar domains and striking electro-optics, *Proceedings of the National Academy of Sciences* **117**, 14021 (2020).
- [13] O. D. Lavrentovich, Ferroelectric nematic liquid crystal, a century in waiting, *Proceedings of the National Academy of Sciences* **117**, 14629 (2020).
- [14] N. Sebastián, M. Čopič, and A. Mertelj, Ferroelectric nematic liquid-crystalline phases, *Physical Review E* **106**, 021001 (2022).
- [15] J. Eckert, B. Ladoux, R.-M. Mège, L. Giomi, and T. Schmidt, Hexanematic crossover in epithelial monolayers depends on cell adhesion and cell density, *Nature Communications* **14**, 5762 (2023).
- [16] J.-M. Armengol-Collado, L. N. Carenza, J. Eckert, D. Krommydas, and L. Giomi, Epithelia are multiscale active liquid crystals, *Nature Physics* **19**, 1773 (2023).
- [17] J.-M. Armengol-Collado, L. N. Carenza, and L. Giomi, Hydrodynamics and multiscale order in confluent epithelia, *Elife* **13**, e86400 (2024).
- [18] R. Bruinsma and G. Aeppli, Hexatic order and herringbone packing in liquid crystals, *Physical Review Letters* **48**, 1625 (1982).
- [19] S. Dierker and R. Pindak, Dynamics of thin tilted hexatic liquid crystal films, *Physical review letters* **59**, 1002 (1987).
- [20] S. Sprunt and J. Litster, Light-scattering study of bond orientational order in a tilted hexatic liquid-crystal film, *Physical review letters* **59**, 2682 (1987).
- [21] J. V. Selinger and D. R. Nelson, Theory of transitions among tilted hexatic phases in liquid crystals, *Physical Review A* **39**, 3135 (1989).
- [22] J. V. Selinger, Dynamics of tilted hexatic phases in liquid-crystal films, *Journal de Physique II* **1**, 1363 (1991).
- [23] V. Drouin-Touchette, P. P. Orth, P. Coleman, P. Chandra, and T. C. Lubensky, Emergent potts order in a coupled hexatic-nematic xy model, *Physical Review X* **12**, 011043 (2022).
- [24] M. Anisimov, E. Gorodetskiĭ, and V. Zaprudskiĭ, Phase transitions with coupled order parameters, *Soviet Physics Uspekhi* **24**, 57 (1981).
- [25] R. B. Meyer, Piezoelectric effects in liquid crystals, *Physical Review Letters* **22**, 918 (1969).
- [26] S. M. Shamid, S. Dhakal, and J. V. Selinger, Statistical mechanics of bend flexoelectricity and the twist-bend phase in bent-core liquid crystals, *Physical Review E—Statistical, Nonlinear, and Soft Matter Physics* **87**, 052503 (2013).
- [27] A. Mertelj, L. Cmok, N. Sebastián, R. J. Mandle, R. R. Parker, A. C. Whitwood, J. W. Goodby, and M. Čopič, Splay nematic phase, *Physical Review X* **8**, 041025 (2018).
- [28] N. Sebastián, L. Cmok, R. J. Mandle, M. R. de la Fuente, I. Drevenšek Olenik, M. Čopič, and A. Mertelj, Ferroelectric-ferroelastic phase transition in a nematic liquid crystal, *Physical review letters* **124**, 037801 (2020).
- [29] M. P. Rosseto and J. V. Selinger, Theory of the splay nematic phase: single versus double splay, *Physical Review E* **101**, 052707 (2020).
- [30] L. Paik and J. V. Selinger, Flexoelectricity versus electrostatics in polar nematic liquid crystals, *arXiv preprint arXiv:2408.10347* (2024).
- [31] S. E. Korshunov, Possible splitting of a phase transition in a $2d$ xy model, *JETP Lett.* **41**, 216 (1985).
- [32] D. Lee and G. Grinstein, Strings in two-dimensional classical xy models, *Physical review letters* **55**, 541 (1985).
- [33] D. Carpenter and J. Chalker, The phase diagram of a generalised xy model, *Journal of Physics: Condensed Matter* **1**, 4907 (1989).
- [34] Y. Shi, A. Lamacraft, and P. Fendley, Boson pairing and unusual criticality in a generalized xy model, *Physical review letters* **107**, 240601 (2011).
- [35] A. Amiri, R. Mueller, and A. Doostmohammadi, Unifying polar and nematic active matter: emergence and co-existence of half-integer and full-integer topological defects, *Journal of Physics A: Mathematical and Theoretical* **55**, 094002 (2022).
- [36] I. Ruider, K. Thijssen, D. R. Vannier, V. Paloschi, A. Sciortino, A. Doostmohammadi, and A. R. Bausch, Topological excitations govern ordering kinetics in endothelial cell layers, *bioRxiv* 10.1101/2024.09.26.615134 (2024), <https://www.biorxiv.org/content/early/2024/09/26/2024.09.26.615134>.
- [37] W. E. Schiesser, *The numerical method of lines: integration of partial differential equations* (Elsevier, 2012).
- [38] W. Press, B. Flannery, S. Teukolsky, and W. Vetterling, Multistep, multivalued, and predictor-corrector methods, *Numerical Recipes in FORTRAN: The Art of Scientific Computing*, 740 (1992).

Supplementary Material

Phase diagram

Here we minimize \mathcal{F} , given by

$$\mathcal{F} = \mathcal{A}_{NP}(Q - p^2)^2 + \mathcal{A}_P p^2 + (Q^2 - 1)^2 \quad (\text{S.1})$$

Setting derivatives of \mathcal{F} to zero, we have

$$\frac{\partial \mathcal{F}}{\partial p} = 0 \implies -2\mathcal{A}_{NP}p(Q - p^2) + \mathcal{A}_P p = 0 \quad (\text{S.2})$$

$$\frac{\partial \mathcal{F}}{\partial Q} = 0 \implies \mathcal{A}_{NP}(Q - p^2) + 2Q(Q^2 - 1) = 0 \quad (\text{S.3})$$

By inspection, $p = 0$ is a solution when $Q = 0$ or $Q = \sqrt{1 - \frac{\mathcal{A}_{NP}}{2}}$ for $\mathcal{A}_{NP} \leq 2$. We now determine which solution gives lower energy for $\mathcal{A}_{NP} < 2$. Substituting into \mathcal{F} , we find

$$\mathcal{F}(p = 0, Q = 0) = 1 \quad (\text{S.4})$$

$$\mathcal{F}\left(p = 0, Q = \sqrt{1 - \frac{\mathcal{A}_{NP}}{2}}\right) = -\frac{1}{4}(\mathcal{A}_{NP} - 4)\mathcal{A}_{NP} \quad (\text{S.5})$$

By inspection, for $\mathcal{A}_{NP} \geq 2$, $1 \geq -\frac{1}{4}(\mathcal{A}_{NP} - 4)\mathcal{A}_{NP}$, with equality for $\mathcal{A}_{NP} = 2$. Thus now the possible solutions are

1. $p = 0$ and $Q = 0$ for $\mathcal{A}_{NP} \geq 2$
2. $p = 0$ and $Q = \sqrt{1 - \frac{\mathcal{A}_{NP}}{2}}$ for $\mathcal{A}_{NP} \leq 2$.

We now look for non-zero p solution. We have

$$\frac{\partial \mathcal{F}}{\partial p} = 0 \implies -2\mathcal{A}_{NP}(Q - p^2) + \mathcal{A}_P = 0 \quad (\text{S.6})$$

$$\frac{\partial \mathcal{F}}{\partial Q} = 0 \implies \mathcal{A}_{NP}(Q - p^2) + 2Q(Q^2 - 1) = 0 \quad (\text{S.7})$$

From the first equation, we learn that

$$Q = p^2 + \frac{\mathcal{A}_P}{2\mathcal{A}_{NP}} \quad (\text{S.8})$$

Thus the nematic order Q is locked to the polar order p , and when this is the case, the nematic order can be written in terms of polar order, which means that half-integer defects are no longer allowed. We will keep in mind that in order for this solution to be valid, we must have $Q > \mathcal{A}_P/(2\mathcal{A}_{NP})$.

Now substituting for p in the 2nd equation gives

$$Q^3 - Q + \frac{\mathcal{A}_P}{4} = 0. \quad (\text{S.9})$$

Since $\mathcal{A}_P/4 > 0$, by Vieta's formula, provided that the discriminant $\Delta = -(27/16)(\mathcal{A}_P^2 - 64/27) \geq 0$, i.e., $\mathcal{A}_P \leq 8/\sqrt{27}$, the only positive solutions for Q are

$$Q = 2 \operatorname{Re} \left[\sqrt[3]{-\frac{\mathcal{A}_P}{8} + i\sqrt{|D|}} \right], \quad 2 \operatorname{Re} \left[e^{4\pi i/3} \sqrt[3]{-\frac{\mathcal{A}_P}{8} + i\sqrt{|D|}} \right], \quad (\text{S.10})$$

where $D = -\Delta/(4 \times 27)$.

It can be shown that \mathcal{F} is smaller when the first solution is taken. This solution is valid when Eq. (S.8) is satisfied, which in terms of \mathcal{A}_P and \mathcal{A}_{NP} , becomes

$$\mathcal{A}_{NP} \geq \frac{\mathcal{A}_P}{2Q} = \mathcal{A}_P / \left(4 \operatorname{Re} \left[\sqrt[3]{-\frac{\mathcal{A}_P}{8} + i\sqrt{|D|}} \right] \right) \quad (\text{S.11})$$

Thus to summarize, the solution is

$$Q = 2 \operatorname{Re} \left[\sqrt[3]{-\frac{\mathcal{A}_P}{8} + i\sqrt{|D|}} \right] \quad (\text{S.12})$$

with $D = -1/27 + \mathcal{A}_P^2/64$, provided that $\mathcal{A}_P \leq 8/\sqrt{27}$ and $Q \geq \mathcal{A}_P/(2\mathcal{A}_{NP})$.

To summarize what we have learned so far, we have three phases:

1. Isotropic phase: $p = 0$ and $Q = 0$ for $\mathcal{A}_{NP} \geq 2$.
2. Nematic phase: $p = 0$ and $Q = \sqrt{1 - \mathcal{A}_{NP}/2}$ for $\mathcal{A}_{NP} \leq 2$.
3. Nematopolar phase: $p = \sqrt{Q - \mathcal{A}_P/(2\mathcal{A}_{NP})}$ and $Q = 2 \operatorname{Re} \left[\sqrt[3]{-\frac{\mathcal{A}_P}{8} + i\sqrt{|D|}} \right]$, with $D = -1/27 + \mathcal{A}_P^2/64$, provided that $\mathcal{A}_P \leq 8/\sqrt{27}$ and $Q \geq \mathcal{A}_P/(2\mathcal{A}_{NP})$.

Now that we have identified the phases, we find the boundaries. We first determine the boundary between the nematic and nematopolar phases. The phase boundary is the curve $\mathcal{A}_P(\mathcal{A}_{NP})$ for $\mathcal{A}_{NP} \leq 2$ such that

$$\mathcal{F} \left(p = 0, Q = \sqrt{1 - \mathcal{A}_{NP}/2} \right) = \mathcal{F} \left(p = \sqrt{Q - \mathcal{A}_P/(2\mathcal{A}_{NP})}, Q = 2 \operatorname{Re} \left[\sqrt[3]{-\frac{\mathcal{A}_P}{8} + i\sqrt{|D|}} \right] \right) \quad (\text{S.13})$$

where $D = -1/27 + \mathcal{A}_P^2/64$. The phase boundary is continuous if the fields p and Q match in both phases, and discontinuous otherwise. The phase boundary is continuous if $p = 0$, which implies $Q = \mathcal{A}_P/(2\mathcal{A}_{NP}) = \sqrt{1 - \mathcal{A}_{NP}/2}$, leading to

$$\mathcal{A}_P(\mathcal{A}_{NP}) = 2\mathcal{A}_{NP}\sqrt{1 - \mathcal{A}_{NP}/2} \quad (\text{S.14})$$

Note that since $\mathcal{A}_P(\mathcal{A}_{NP} = 4/3) = 8/\sqrt{27}$, the continuous part of the phase boundary has endpoints at $(\mathcal{A}_P, \mathcal{A}_{NP}) = (0, 0)$ and $(\mathcal{A}_P, \mathcal{A}_{NP}) = (8/\sqrt{27}, 4/3)$. Hence the point $(\mathcal{A}_P, \mathcal{A}_{NP}) = (8/\sqrt{27}, 4/3)$ is a tricritical point, where a continuous and a discontinuous phase transition meet.

We now need to determine the continuation of the boundary from $\mathcal{A}_{NP} = 4/3$ to $\mathcal{A}_{NP} = 2$. We first note that

$$\mathcal{F} \left(p = \sqrt{Q - \mathcal{A}_P/(2\mathcal{A}_{NP})}, Q \right) = -\frac{1}{4} \frac{\mathcal{A}_P^2}{\mathcal{A}_{NP}} + \mathcal{A}_P Q + (Q^2 - 1)^2. \quad (\text{S.15})$$

Substituting Eqs. (S.5) and (S.15) into Eq. (S.13), we find that

$$-\frac{1}{4} \mathcal{A}_{NP}(\mathcal{A}_{NP} - 4) = -\frac{1}{4} \frac{\mathcal{A}_P^2}{\mathcal{A}_{NP}} + \mathcal{A}_P Q + (Q^2 - 1)^2. \quad (\text{S.16})$$

Upon multiplication by $4\mathcal{A}_{NP}$ and rearrangement, we arrive at

$$\mathcal{A}_{NP}^3 - 4\mathcal{A}_{NP}^2 + [4\mathcal{A}_P Q + 4(Q^2 - 1)^2] \mathcal{A}_{NP} - \mathcal{A}_P^2 = 0. \quad (\text{S.17})$$

Recalling that Q is independent of \mathcal{A}_{NP} , then we have a cubic equation for \mathcal{A}_{NP} , which we now solve.

Upon the following change of variables from \mathcal{A}_{NP} to $\tilde{\mathcal{A}}_{NP}$ given by

$$\mathcal{A}_{NP} = \tilde{\mathcal{A}}_{NP} + 4/3, \quad (\text{S.18})$$

we now need to solve

$$\tilde{\mathcal{A}}_{NP}^3 + a\tilde{\mathcal{A}}_{NP} + b = 0 \quad (\text{S.19})$$

where

$$a = 4(\mathcal{A}_P Q + (Q^2 - 1)^2) - \frac{16}{3} \quad (\text{S.20})$$

$$b = -\frac{128}{27} + \frac{16}{3}(\mathcal{A}_P Q + (Q^2 - 1)^2) - \mathcal{A}_P^2, \quad (\text{S.21})$$

and Q is given by Eq. (S.12).

We note that since we can express the discriminant Δ as

$$\Delta = -(4 \times 27) \left(Q^3 - Q + \frac{\mathcal{A}_P}{4} \right) \left(-\frac{64}{27} Q^3 + \frac{64}{27} Q - \frac{32}{27} \mathcal{A}_P + \frac{16}{3} \mathcal{A}_P Q^2 - 4\mathcal{A}_P^2 Q + \mathcal{A}_P^3 \right), \quad (\text{S.22})$$

then since Q satisfies Eq. (S.9), $\Delta = 0$. Hence,

$$\mathcal{A}_{NP} = \tilde{\mathcal{A}}_{NP} + 4/3 = 2 \left(-\frac{b}{2} \right)^{1/3} + 4/3 \quad (\text{S.23})$$

In the limit $\mathcal{A}_{NP} \gg 1$, we have $p = 0$, and hence the boundary for large \mathcal{A}_{NP} asymptotes to $\mathcal{A}_P = 4\sqrt{6}/9$, which is obtained by solving the systems of equations

$$\mathcal{F}(p = 0, Q) = 1 \quad (\text{S.24})$$

$$\left. \frac{\partial \mathcal{F}}{\partial Q} \right|_{p=0} = 0 \quad (\text{S.25})$$

for Q and \mathcal{A}_P .

We now determine the phase boundary between the nematopolar and isotropic phases. Since in the nematopolar phase, we cannot have both p and Q vanish, then the phase boundary between the nematopolar and isotropic phases is a discontinuous phase transition. The phase boundary is determined by

$$\mathcal{F}(p = 0, Q = 0) = \mathcal{F} \left(p = \sqrt{Q - \mathcal{A}_P/(2\mathcal{A}_{NP})}, Q = 2 \operatorname{Re} \left[\sqrt[3]{-\frac{\mathcal{A}_P}{8} + i\sqrt{|D|}} \right] \right), \quad (\text{S.26})$$

where $D = -1/27 + \mathcal{A}_P^2/64$. Recalling that $\mathcal{F}(0, 0) = 1$, and using Eq. (S.15), we have

$$1 = -\frac{1}{4} \frac{\mathcal{A}_P^2}{\mathcal{A}_{NP}} + \mathcal{A}_P Q + (Q^2 - 1)^2 \quad (\text{S.27})$$

and hence the phase boundary is determined by

$$\mathcal{A}_{NP} = \frac{\mathcal{A}_P^2}{4(\mathcal{A}_P Q + (Q^2 - 1)^2 - 1)}, \quad (\text{S.28})$$

where Q satisfies Eq. (S.12).

Finally, the triple point, where all three phases meet, is at $(\mathcal{A}_P, \mathcal{A}_{NP}) = (\sqrt{2}, 2)$, which is when

$$\mathcal{F}(p = 0, Q = 0) = \mathcal{F}(p = 0, Q = \sqrt{1 - \mathcal{A}_{NP}/2}) = \mathcal{F} \left(p = \sqrt{Q - \mathcal{A}_P/(2\mathcal{A}_{NP})}, Q = 2 \operatorname{Re} \left[\sqrt[3]{-\frac{\mathcal{A}_P}{8} + i\sqrt{|D|}} \right] \right), \quad (\text{S.29})$$

where $D = -1/27 + \mathcal{A}_P^2/64$.

Related model

A related model, the polarnematic model, where the roles of \vec{p} and \overleftrightarrow{Q} are reversed, that is, \vec{p} is ordered whereas \overleftrightarrow{Q} is isotropic, has the following free energy:

$$\mathcal{F} = \mathcal{A}_{NP} \left| \overleftrightarrow{Q} - \overleftrightarrow{P} \right|^2 + \mathcal{A}_P |Q|^2 + (|p|^2 - 1)^2. \quad (\text{S.30})$$

\mathcal{F} is minimized when \overleftrightarrow{Q} and \overleftrightarrow{P} are aligned. In terms of the magnitudes Q and p of \overleftrightarrow{Q} and \vec{p} , respectively, \mathcal{F} becomes

$$\mathcal{F} = \mathcal{A}_{NP}(Q - p^2)^2 + \mathcal{A}_P Q^2 + (p^2 - 1)^2, \quad (\text{S.31})$$

which is minimized when

$$p = \sqrt{\frac{\mathcal{A}_P + \mathcal{A}_{NP}}{\mathcal{A}_P + \mathcal{A}_{NP} + \mathcal{A}_P \mathcal{A}_{NP}}} \quad (\text{S.32})$$

$$Q = \frac{\mathcal{A}_{NP}}{\mathcal{A}_P + \mathcal{A}_{NP} + \mathcal{A}_P \mathcal{A}_{NP}}. \quad (\text{S.33})$$

This model is much simpler as there is only one phase: the polar field always orders the nematic field. For the remainder of this paper, we focus on the nematopolar model where the nematic field prefers to be oriented and the polar field prefers to be isotropic.

Critical exponents

For a magnetization m , the critical exponents α , β , and γ are defined by specific heat $C \equiv -T \frac{\partial^2 \mathcal{F}}{\partial T^2} \propto (T - T^*)^{-\alpha}$, magnetization $m \propto (T - T^*)^\beta$, and susceptibility $\chi \equiv \frac{\partial m}{\partial h} \Big|_{h=0} \propto (T - T^*)^{-\gamma}$, respectively, where h is external field. For the N-I line, we assume $2 - \mathcal{A}_{NP} \approx T^* - T$, and for the N-NP curve, we assume $\mathcal{A}_P^* - \mathcal{A}_P \approx T - T^*$. For the N-I line, the magnetization $m = Q$, and thus it is just the usual mean-field Ising model, so $\alpha = 0$, $\beta = 1/2$, and $\gamma = 1$.

Recall that the free energy \mathcal{F} is

$$\mathcal{F} = \mathcal{A}_{NP}(Q - p^2)^2 + \mathcal{A}_P p^2 + (1 - Q^2)^2. \quad (\text{S.34})$$

We first find the critical exponents for the N-I line. Here, Q is the magnetization, and $p = 0$. The free energy becomes

$$\mathcal{F} = \mathcal{A}_{NP} Q^2 + (1 - Q^2)^2. \quad (\text{S.35})$$

where we assume $\mathcal{A}_{NP}^* - \mathcal{A}_{NP} \approx T^* - T$. This is simply the usual mean-field Ising model with the associated critical exponents.

For the N-NP curve, we have two different analogs of magnetizations: p , and the locking order parameter $\sigma \equiv Q - p^2 - \frac{\mathcal{A}_P}{2\mathcal{A}_{NP}}$. We show here that generically, the critical exponents for p are $\alpha = 0$, $\beta = 1/2$, and $\gamma = 1$, and at the tricritical point $(\mathcal{A}_P, \mathcal{A}_{NP}) = (8/\sqrt{27}, 4/3)$, the critical exponents for p shift to $\alpha = 1$, $\beta = 1/4$, and $\gamma = 1/2$. For σ , the critical exponents are $\alpha = 0$, $\beta = 1$, and $\gamma = 0$.

Recall that in the nematic phase, we have

$$p = 0, \quad Q = \sqrt{1 - \mathcal{A}_{NP}/2} \quad (\text{S.36})$$

and in the nematopolar phase, we have

$$p = \sqrt{Q - \frac{\mathcal{A}_P}{2\mathcal{A}_{NP}}}, \quad Q = Q(\mathcal{A}_P) \neq 0 \quad (\text{S.37})$$

We now find the critical exponents for the N-NP curve. Here, we have two choices of magnetization: p , or σ . We first

consider p for magnetization. Then the free energy becomes

$$\mathcal{F} = \mathcal{A}_{NP}(Q - p^2)^2 + \mathcal{A}_P p^2 + (1 - Q^2)^2 - hp, \quad (\text{S.38})$$

where we assume $\mathcal{A}_P^* - \mathcal{A}_P \approx T - T^*$ and we coupled p to external field h .

We first consider a generic point on N-NP curve (excluding the tricritical point). We find β by recalling that in the nematopolar phase, since Q is independent of \mathcal{A}_{NP} , then

$$p = \sqrt{Q - \frac{\mathcal{A}_P}{2\mathcal{A}_{NP}}} \sim \sqrt{\mathcal{A}_P^* - \mathcal{A}_P} \quad (\text{S.39})$$

giving $\beta = 1/2$. By inspection, it follows that $T \frac{\partial^2 \mathcal{F}}{\partial T^2} \approx 1$, giving $\alpha = 0$. The hyperscaling relation $\alpha + 2\beta + \gamma = 1$ implies that $\gamma = 1$.

We now evaluate the critical exponents at the tricritical point. Since at the tricritical point, $\frac{\partial^2 \mathcal{F}}{\partial Q^2} = 0$, we also have $Q - Q_c \approx \sqrt{\mathcal{A}_P^* - \mathcal{A}_P}$, which from $Q = \sqrt{p^2 - \frac{\mathcal{A}_P}{2\mathcal{A}_{NP}}}$ leads to $p \approx (\mathcal{A}_P^* - \mathcal{A}_P)^{1/4}$, and thus $\beta = 1/4$. Also, by the chain rule, we can write

$$\frac{\partial^2 \mathcal{F}}{\partial \mathcal{A}_P^2} = \frac{\partial Q}{\partial \mathcal{A}_P} \frac{\partial^2 \mathcal{F}}{\partial Q^2} \quad (\text{S.40})$$

where we have used the fact that $\frac{\partial \mathcal{F}}{\partial Q} = 0$. Thus since $Q - Q_c \approx \sqrt{\mathcal{A}_P^* - \mathcal{A}_P}$ and $\frac{\partial^2 \mathcal{F}}{\partial Q^2} \approx 1$, we find that

$$\frac{\partial^2 \mathcal{F}}{\partial \mathcal{A}_P^2} \approx (\mathcal{A}_P^* - \mathcal{A}_P)^{-1} \quad (\text{S.41})$$

giving $\alpha = 1$. The hyperscaling relation $\alpha + 2\beta + \gamma = 1$ implies that $\gamma = 1/2$.

We now repeat this exercise for σ . We first note that $\beta = 1$, since in the nematic phase, $\sigma = Q - \frac{\mathcal{A}_P}{2\mathcal{A}_{NP}}$, where Q is independent of \mathcal{A}_{NP} .

In the nematic phase, since $p = 0$, the free energy \mathcal{F} becomes

$$F = \mathcal{A}_{NP}Q^2 + (Q^2 - 1)^2, \quad (\text{S.42})$$

and since Q is independent of \mathcal{A}_P , then \mathcal{F} is as well, leading to $\alpha = 0$. The hyperscaling relation $\alpha + 2\beta + \gamma = 1$ implies that $\gamma = 0$.

External fields

We consider the following free energy:

$$\mathcal{F} = \mathcal{A}_{NP} \left| \overleftrightarrow{Q} - \overleftrightarrow{P} \right|^2 + \mathcal{A}_P |p|^2 + (|Q|^2 - 1)^2 - \text{tr} \left[\overleftrightarrow{H} \overleftrightarrow{Q} \right] - \vec{h} \cdot \vec{p}. \quad (\text{S.43})$$

We consider two cases here in order: (i) $\vec{h} = 0, \overleftrightarrow{H} \neq 0$, and (ii) $\vec{h} \neq 0, \overleftrightarrow{H} = 0$.

$$\vec{h} = 0 \text{ and } \overleftrightarrow{H} \neq 0$$

Here we analyze the case of $\vec{h} = 0$ and $\overleftrightarrow{H} \neq 0$. When $\vec{h} = 0$, the free energy \mathcal{F} becomes

$$\mathcal{F} = \mathcal{A}_{NP} \left| \overleftrightarrow{Q} - \overleftrightarrow{P} \right|^2 + \mathcal{A}_P |p|^2 + (|Q|^2 - 1)^2 - \text{tr} \left[\overleftrightarrow{H} \overleftrightarrow{Q} \right] \quad (\text{S.44})$$

which is minimized when $\overleftrightarrow{H}, \overleftrightarrow{Q}$, and \overleftrightarrow{P} are all aligned. Without loss of generality, we choose coordinates x and y such that $H^{xy} = 0$, and thus by suitable choices of rotations, we can assume $Q^{xy} = 0$ and that $p^y = 0$. This leads to

$$\mathcal{F} = \mathcal{A}_{NP}(Q - p^2)^2 + \mathcal{A}_P p^2 + (Q^2 - 1)^2 - 2HQ \quad (\text{S.45})$$

where now Q, p, H denote the magnitudes of Q, p, H . Thus in equilibrium,

$$\frac{\partial \mathcal{F}}{\partial p} = -4\mathcal{A}_{NP}p(Q - p^2) + 2\mathcal{A}_P p = 0 \quad (\text{S.46a})$$

$$\frac{\partial \mathcal{F}}{\partial Q} = 2\mathcal{A}_{NP}(Q - p^2) + 4Q(|Q|^2 - 1) - 2H = 0 \quad (\text{S.46b})$$

From Eq. (S.46)(a), two possible solutions are $p = 0$ and $p \neq 0$. We first consider the case $p = 0$.

$$p = 0$$

We first consider the case $p = 0$. When $p = 0$, Eq. (S.46)(b) reduces to

$$\frac{\partial \mathcal{F}}{\partial Q} = \mathcal{A}_{NP}Q + 2Q(Q^2 - 1) - H = 0 \quad (\text{S.47})$$

Since $H > 0$, the solution of $Q = 0$ is no longer allowed, and thus the N-I phase boundary disappears. In particular, the only non-negative solution is

$$Q = \sqrt[3]{\frac{H}{4} + \sqrt{\frac{1}{27} \left(\frac{\mathcal{A}_{NP}}{2} - 1\right)^3 + \frac{H^2}{16}}} + \sqrt[3]{\frac{H}{4} - \sqrt{\frac{1}{27} \left(\frac{\mathcal{A}_{NP}}{2} - 1\right)^3 + \frac{H^2}{16}}} \quad (\text{S.48})$$

$$p \neq 0$$

We now assume $p \neq 0$. Then Eq. (S.46)(a) simplifies to

$$Q - p^2 = \frac{\mathcal{A}_P}{2\mathcal{A}_{NP}} \quad (\text{S.49})$$

and upon substitution of the above into Eq. (S.46)(b), we learn that

$$\frac{\mathcal{A}_P}{2} + 2Q(Q^2 - 1) - H = 0 \quad (\text{S.50})$$

For sufficiently small H , i.e., $H \leq \mathcal{A}_P/2$, the solution is

$$Q = 2 \operatorname{Re} \left[\sqrt[3]{-\frac{\mathcal{A}_P - 2H}{8} + i\sqrt{|D|}} \right] \quad (\text{S.51})$$

with $D = -\frac{1}{27} + \frac{1}{64}(\mathcal{A}_P - 2H)^2$, provided $\mathcal{A}_P - 2H \leq 8/\sqrt{27}$ and $Q \geq \mathcal{A}_P/(2\mathcal{A}_{NP})$.

We now show that the N-NP phase boundary is deformed, but remains a continuous phase transition. We find the boundary by setting $p = 0$, $Q = \mathcal{A}_P/(2\mathcal{A}_{NP})$, and finding the region of parameter space where these conditions and Eq. (S.46) are satisfied. Doing so gives

$$\frac{\mathcal{A}_P}{2} + \frac{\mathcal{A}_P}{\mathcal{A}_{NP}} \left(\frac{\mathcal{A}_P^2}{4\mathcal{A}_{NP}^2} - 1 \right) = H. \quad (\text{S.52})$$

$$\vec{h} \neq 0 \text{ and } \overleftrightarrow{H} = 0$$

Here we analyze the case of $\vec{h} \neq 0$ and $\overleftrightarrow{H} = 0$. When $\overleftrightarrow{H} = 0$, the free energy \mathcal{F} reduces to

$$\mathcal{F} = \mathcal{A}_{NP} |\overleftrightarrow{Q} - \overleftrightarrow{P}|^2 + \mathcal{A}_P |p|^2 + (|Q|^2 - 1)^2 - \vec{h} \cdot \vec{p}, \quad (\text{S.53})$$

which is minimized when \vec{p} is aligned with \vec{h} , and \vec{Q} is aligned with \vec{P} . Without loss of generality, we choose \vec{h} to point in the \hat{x} direction. p then points in the \hat{x} direction as well, and $Q^{xy} = 0$. This leads to at equilibrium,

$$\frac{\partial \mathcal{F}}{\partial p} = -2\mathcal{A}_{NPP}(Q - p^2) + \mathcal{A}_P p - h = 0 \quad (\text{S.54a})$$

$$\frac{\partial \mathcal{F}}{\partial Q} = \mathcal{A}_{NP}(Q - p^2) + 2Q(Q^2 - 1) = 0 \quad (\text{S.54b})$$

From Eq. (S.54)(a), we see that $p = 0$ is not a solution, and hence from Eq. (S.54)(b), we see that $Q = 0$ is also not a solution. Hence, for non-zero h , the nematic and isotropic phases no longer exist – only the nematopolar phase exists. By continuity, for small deformation h , the two continuous phase transitions disappear.

Numerical details

In our numerical simulations, we minimize the free energy by relaxational dynamics. We do so numerically using the method of lines [37], where the temporal evolution is performed through a predictor-corrector scheme [38] and spatial derivatives are evaluated using five-point stencil central differences. In the absence of an external field, this method led to steady-states, whereas in the presence of an external field, the topological defects moved until they reached the boundary, see Fig. S1 for representative snapshots of movement of the topological defects.

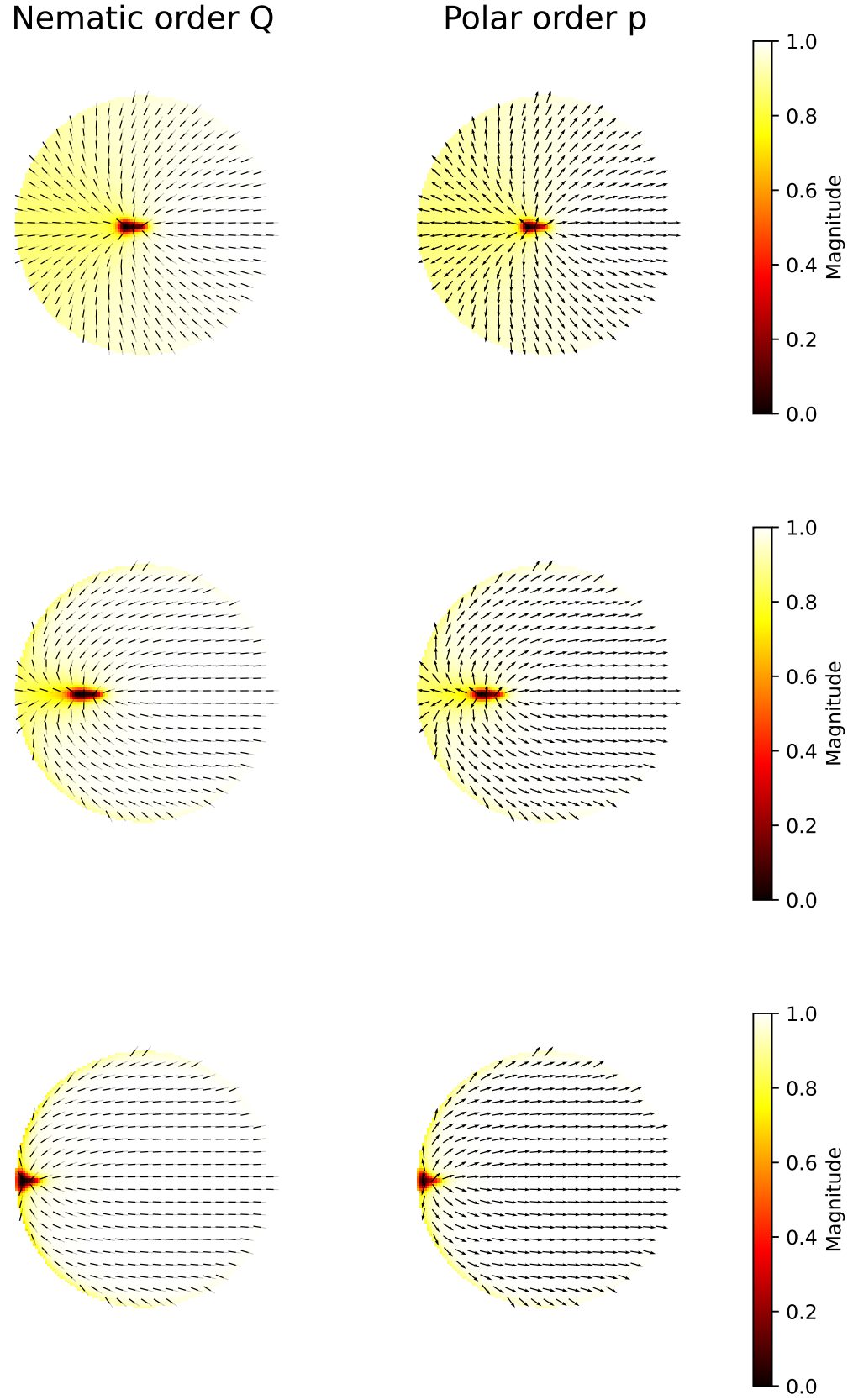


FIG. S1. Key snapshots of simulations of plots of p and Q in tightly locked regime and large external field h , where color denotes the magnitudes. Snapshots in each column are time-ordered from top to bottom. Initially, the topological defects are at the origin, but they are eventually expelled from the bulk and absorbed by the boundary. Parameters used: $\mathcal{A}_P = 1, \mathcal{A}_{NP} = 4, h = 4$.